



Earthquake Prediction Based on Combined Seismic and GPS Monitoring Data

V. G. Gitis^{ID}, A. B. Derendyaev^(✉)^{ID}, and K. N. Petrov^{ID}

The Institute for Information Transmission Problems, Moscow, Russia
gitis@iitp.ru

Abstract. This article presents the results of applying the method of the minimum area of alarm to the complex forecasting of earthquakes based on data of different types. Point fields of earthquake epicenters and time series of displacements of the earth's surface, measured using GPS, were used for the prediction. Testing was carried out for earthquakes with a hypocenter depth of up to 60 km for two regions with different seismotectonics: Japan, the forecast time interval from 2016 to 2020, magnitudes $m \geq 6$; California, the forecast time interval from 2013 to 2020, magnitude $m \geq 5.5$. Testing has shown the effectiveness of systematic earthquake forecasting using seismological and space geodesy data in combination.

Keywords: GPS time series · Grid-based spatio-temporal fields · Earthquake prediction · Machine learning · Method of minimum area of alarm

1 Introduction

Field observations show that anomalous changes are observed in a number of natural processes before a strong earthquake. They can relate to the characteristics of the seismic regime, the values of deformations of the earth's surface, the chemical composition of fluids, the level of groundwater, the transit time of seismic waves, variations of electric and geomagnetic fields. These phenomena are often localized near the source of a future earthquake [11, 14, 18, 20, 26, 27] and can be used as precursors of earthquakes. At the same time, it is known that with an increase in the energy of the expected earthquake, the distance from the epicenter to the area of manifestation of precursors increases and can be more than 15 km [4, 10], which introduces additional uncertainty in the assessment of the location of the expected earthquake.

Many aspects of earthquake prediction have been studied. They include the study of rock failure and earthquake precursor phenomena, the study of mathematical models for earthquake prediction, machine learning methods, and the

This research was partially funded by Russian Foundation for Basic Research grant number 20-07-00445.

testing of earthquake prediction algorithms [12, 16, 23–25, 29, 30]. At the same time, a number of works have stated that earthquakes cannot be predicted [6, 9, 15].

Systematic earthquake prediction consists of the regular calculation of a limited warning zone, in which an earthquake with a magnitude above a certain threshold is expected for a certain time. The effectiveness of the forecast largely depends on the quality of the initial data and methods of their processing. We get the broadest access to regularly updated seismological monitoring data. Therefore, as a rule, in many articles, only seismological data are used. Currently, data from monitoring the displacement of the earth's surface, obtained using a global positioning system (GPS), is published in real-time for a number of seismically active regions.

In this article, we consider the results of a systematic forecast obtained with the combined use of seismological and geodynamic data. For the systematic prediction of earthquakes, we have developed a new method of machine learning, called the method of the minimum area of alarm [8]. The article is divided into three sections. In Sect. 2, we shortly describe the main elements of the forecast method. Section 3 presents the results of modeling the forecast of strong earthquakes in Japan and California, obtained on the basis of combining seismic and geodetic data.

2 Basis of a Forecasting Method

The considered approach to the systematic forecasting of earthquakes is based on the machine learning method, which we called the method of the minimum area of alarm. This method is described in [7, 8]. The idea of the method is as follows.

Let there be a set of objects. An object is described by a set of its properties, expressed in numerical form (a vector of features). The values of the properties of objects, close to the maximum possible, have a low probability. Among the set of objects, there are anomalous objects (precedents). They differ from other objects in that the values of some of their properties are close to the maximum. It seems natural to classify an object as anomalous if the corresponding feature vector is greater than or equal componentwise to one of the vectors corresponding to the precedent. However, the description of the properties of objects is usually incomplete. Therefore, some precedents lack properties that are close to their maximum values. For such precedents, the number of objects classified by them as anomalous can be quite large, and the objects themselves are likely to be erroneously classified as anomalous.

The task is to find the largest number of precedents, provided that the number of objects classified by them as anomalous does not exceed the specified number. The algorithm of the minimum area of alarm is non-parametric. It refers to machine learning algorithms for one-class classification [2, 13, 17]. The idea of the algorithm is as follows. At the first step, for each precedent, a set of anomalous objects classified by it is built. Next, the maximum number of

precedents is selected for which the cardinality of the union of these sets does not exceed a predetermined number N^* . The decision rule classifies objects only according to the selected precedents. For the rest of the precedents, new distinctive properties should be sought and added to the feature space. The amount of computations of the algorithm is significantly reduced if not the maximum number of precedents is selected, but a close one.

With a systematic forecast of earthquakes, it is required to regularly indicate on the map the alarm zone, in which the epicenter of the target earthquake is expected. A demo version of the systematic earthquake prediction system since 2018 is available on the website <https://distcomp.ru/geo/prognosis/> (accessed on 15 March 2021). At each step Δt , new initial data are loaded from the seismological and geodynamic monitoring servers, they are used to calculate the spatial and spatio-temporal grid-based fields, the sample of target earthquake epicenters is supplemented, and then training is performed with all downloaded data from the beginning of training until the moment of forecasting t . As a result of training, an alarm zone with size $S^*(t)$ is calculated, in which the epicenter of the target earthquake is expected in the interval $(t, t + \Delta t)$.

A target earthquake is predicted if its epicenter falls within the calculated alarm zone. The larger the product $S^*(t)\Delta t$, the more successful the forecast. At the same time, it is obvious that the size of this region of space-time must be reasonably limited. Indicators of forecast quality are the assessment of the probability of a successful forecast of events (*forecast probability*), equal to $U = Q^*/Q$ and the *alarm volume* equal to $V = L^*/L$, where Q^* and Q are the number of predicted and all target earthquakes, $L^* = \Delta t \sum_{n=1}^N S^*(t_n)$ is the size of the spatio-temporal area of alarm, N is the number of forecast intervals, $L = NS\Delta t$ is the size of the entire analysis spatio-temporal area, S is the size of the analysis zone. As a result of training, it is desirable to obtain a solution that provides the maximum probability of a successful prediction for a given value of the alarm area. It can be seen that the alarm volume V is equal to the probability of detecting target events by random areas of size $L^* = VL$.

3 Modeling

3.1 GPS Data Preprocessing

We analyzed the time series of daily horizontal displacements of the earth's surface at the intervals 01.01.2009–26.07.2020 for Japan and 01.01.2008–14.11.2020 for California. The data obtained from the Nevada Geodetic Laboratory (NGL), <http://geodesy.unr.edu/about.php> (accessed on 15 March 2021) [3]. There are 1420 and 1803 GPS receiving stations in Japan and California, respectively. The analysis areas contain 1229 and 1204 stations. Networks of GPS receiving stations, areas of analysis, and epicenters of target earthquakes are shown in Fig. 1. Stations evenly cover the analysis area. The average minimum distance between stations is 12.8 km for Japan and 9.38 km for California, with standard deviations of 5.4 and 5.74 km.

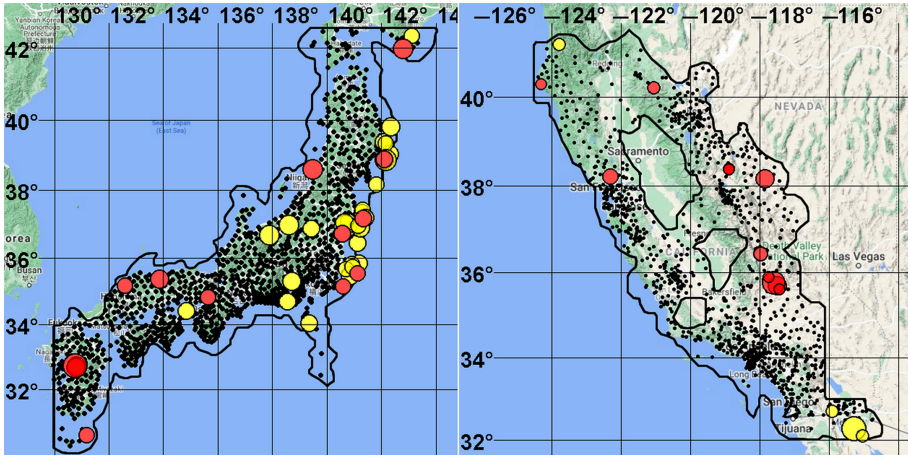


Fig. 1. Areas of analysis, Global Positioning System (GPS) ground receiving stations, and the epicenters of target earthquakes. Left: Japan, epicenters of target earthquakes with magnitude $m \geq 6.0$ in the interval 01.01.2011–26.07.2020; Right: California, epicenters of target earthquakes with magnitude $m \geq 5.5$, in the interval 23.12.2009–14.11.2020. The epicenters of the target earthquakes for which the forecast was tested are highlighted in red. (Color figure online)

The calculation of the feature fields used for earthquake prediction based on GPS data is performed in two stages. The purpose of the first stage is to extract a useful signal from the time series of coordinates of the receiving stations. The purpose of the second stage is to calculate spatio-temporal fields of forecast features.

Time Series of Earth's Surface Displacement Velocities

The initial data are daily time series of coordinates $x(t)$ and $y(t)$ of GPS ground receiving stations in the W–E and N–S directions in the intervals 01.01.2009–26.07.2020 for Japan and 01.01.2008–14.11.2020 for California. The daily horizontal velocities of the earth's surface displacements $g_x(t)$ and $g_y(t)$ are determined by two coordinates of the GPS receiving station, spaced in time by the interval T_0 : $g_x(t) = (x(t) - x(t - T_0))/T_0$, $g_y(t) = (y(t) - y(t - T_0))/T_0$. There are discontinuities (gaps) in the time series. In our case, for each coordinate, there were 23682 gaps and 168218 days of missed measurements for Japan, and 29977 gaps and 357067 days of missed measurements for California. Since the displacement rate estimates are ahead of the time of the values of the first station coordinates $x(t - T_0)$ and $y(t - T_0)$ by T_0 days, each gap in the time series of station coordinates increases the number of missing values in the time series of velocities by T_0 days. With a large number of gaps, the number of missing velocity values can significantly exceed the number of missing coordinate values. To limit the number of missed velocity values, we linearly interpolate the coordinate values in the gaps less than or equal to T_0 . For the gaps that more than T_0 days,

we end the calculation of the speed at the last value of the station coordinate before the start of the rupture and re-estimate the rates, starting from the first value of the station coordinate after the rupture.

To calculate the daily rates, we selected the interval $T_0 = 30$ days. For this interval, the station movement values are comparable to the noise value of daily measurements. For 30 days intervals, there are 23119 gaps in each coordinate of the Japan area, which is 97.62% of all gaps in the time series and 50537 blanks in measurements (30.04%). For California, there are 27990 measurement gaps (93.37%) and 88387 measurement gaps (24.75%) over a 30-day period for each coordinate. At the same time, the number of missing speed values in each of the W–E and N–S directions increased for Japan by $(23682 - 23119) \times 30 = 16890$ (10.04%), and for California by $(29977 - 27990) \times 30 = 59610$ (16.69%).

The first stage is completed by calculating the spatio-temporal fields of the rate components \mathbf{V}_x and \mathbf{V}_y in the W–E and N–S directions. The fields were presented in the grid $\Delta x \times \Delta y \times \Delta t = 0.1^\circ \times 0.075^\circ \times 1$ day. The calculation of the fields was carried out using an interpolation technique known as inverse distance weighting. During interpolation, the gaps in the values of the time series were not filled, but they were taken into account as the absence of the receiving station. The values of the fields \mathbf{V}_x and \mathbf{V}_y at the grid points for each time slice of the field of the velocity component W–E were calculated by the formula:

$$V_{xn}(t) = \frac{\sum_{k=1}^K g_{xk}^{(t)} / r_k^p}{\sum_{k=1}^K 1 / r_k^p}, \tag{1}$$

where $V_{xn}(t)$ is the value of the field of the W–E strain rate component at the grid node n at the moment t , K is the maximum number of stations closest to the node n in the circle of radius R_{max} , the values of which were used for interpolation, $g_{xk}(t)$ is the value of the W–E strain rate component for the station $k, k = 1, \dots, K$, at the time t , $r_k \leq R_{max}$ is the distance from the k -th station to the grid node n , and p is the degree that determines the dependence of the station weight on its distance to the grid node. The interpolation parameters were $K = 5$, $R_{max} = 50$ km, and $p = 1$. If $r_k = 0$, then $V_{xn}(t) = g_{xk}(t)$. The calculations of the field of the N–S strain rate components were similar.

Spatio-temporal Fields of Features

We assume that strong earthquakes are preceded by spatio-temporal anomalous changes in the regime of various deformations of the earth’s surface. Therefore, we are looking for fields containing information about the anomalous values of the change in the deformation mode. The basis of the considered fields of features is the following invariants of the strain-rate fields.

- \mathbf{F}_1 is the field of divergence of the strain rates:

$$\text{div}V_n = \frac{\partial V_{xn}}{\partial x} + \frac{\partial V_{yn}}{\partial y} \tag{2}$$

The maximum and minimum values of the divergence field refer to places where there is a relative contraction or expansion of the size of a small horizontal area.

– \mathbf{F}_2 is the field of rotor of the strain rates:

$$\text{rot}V_n = \frac{\partial V_{xn}}{\partial y} - \frac{\partial V_{yn}}{\partial x} \tag{3}$$

The field values determine the direction and intensity of the field twisting around the vertical axis.

– \mathbf{F}_3 is the field of shear of the strain rates:

$$\text{sh}V_n = \frac{1}{2} \sqrt{\left(\frac{\partial V_{xn}}{\partial x} - \frac{\partial V_{yn}}{\partial y}\right)^2 + \left(\frac{\partial V_{xn}}{\partial y} + \frac{\partial V_{yn}}{\partial x}\right)^2} \tag{4}$$

The fields of features \mathbf{F}_4 , \mathbf{F}_5 , and \mathbf{F}_6 represent changes in the fields of the strain rate invariants over time. They are equal to the ratios of the mean values of the invariants in two consecutive intervals to the standard deviation of this difference. The values of the fields are converted into the grid $\Delta x \times \Delta y \times \Delta t = 0.1^\circ \times 0.075^\circ \times 30$ days.

– \mathbf{F}_4 is the field of the temporal variations in the divergence strain rate.

The value of the field $f_{4n}(t)$ at time t is equal to the ratio of the difference $(\overline{\text{div}_{2n}} - \overline{\text{div}_{1n}})$ between the mean values of the divergence in two consecutive intervals, namely, T_1 and T_2 , to the standard deviation of this difference $\sigma_n(\text{div})$, $T_1 = T_2 = 361$ days.

$$f_{4n}(t) = (\overline{\text{div}_{2n}} - \overline{\text{div}_{1n}}) / \sigma_n(\text{div}), \tag{5}$$

where $\overline{\text{div}_{2n}}$ is calculated from the values of field \mathbf{F}_1 at the interval $(t - T_2, t)$, $\overline{\text{div}_{1n}}$ is calculated at the interval $(t - T_2 - T_1, t - T_2)$.

– \mathbf{F}_5 is the field of the temporal variations in the rotor rate.

The values of field $f_5(t)$ are calculated similarly to the values of field \mathbf{F}_4 ,

$$f_{5n}(t) = (\overline{\text{rot}_{2n}} - \overline{\text{rot}_{1n}}) / \sigma_n(\text{rot}). \tag{6}$$

– \mathbf{F}_6 is the field of the temporal variations in the shear deformation rate.

The values of field $f_6(t)$ are calculated similarly to the values of field \mathbf{F}_4 ,

$$f_{6n}(t) = (\overline{\text{sh}_{2n}} - \overline{\text{sh}_{1n}}) / \sigma_n(\text{sh}), \tag{7}$$

Fields \mathbf{F}_7 , \mathbf{F}_8 , and \mathbf{F}_9 represent spatial correlations of strain rate changes in a sliding window of 75×75 km². With this window size, the correlation coefficients are estimated in approximately 70–80 grid points of the fields.

- \mathbf{F}_7 is the field of spatial correlations in fields \mathbf{F}_4 and \mathbf{F}_5 .
- \mathbf{F}_8 is the field of spatial correlations in fields \mathbf{F}_4 and \mathbf{F}_6 .
- \mathbf{F}_9 is the field of spatial correlations in fields \mathbf{F}_5 and \mathbf{F}_6 .

Correlation fields \mathbf{F}_7 , \mathbf{F}_8 , and \mathbf{F}_9 carry information about the spatial relationship between the values of the change in the rate of different pairs of deformation types. The minimum or maximum fields of the correlation fields combine this information.

To combine information on the spatial relationship between the values of the change in the rate of different pairs of deformation types, you can use the field of maximum or minimum values of the correlation fields \mathbf{F}_7 , \mathbf{F}_8 , and \mathbf{F}_9 . This operation can be interpreted in terms of fuzzy logic [28]. For Japan, the most successful prediction of target earthquakes was obtained using the \mathbf{F}_{10} field:

- \mathbf{F}_{10} is the field of minimum values of the fields \mathbf{F}_7 and \mathbf{F}_9 :

$$f_{10n} = \min(f_{7n}, f_{9n}) \quad (8)$$

The best forecast of target earthquakes according to GPS data for California was obtained from the \mathbf{F}_4 and \mathbf{F}_6 fields.

3.2 Seismological Data Preprocessing

Seismological data for Japan and California taken from the Japan Meteorological Agency earthquake catalogs [21, 22] and the National Earthquake Information Center (NEIC) [1] at intervals 02.06.2002–26.07.2020 and 01.01.1995–20.12.2020. They are represented by earthquakes with a magnitude $m \geq 2.0$ and a hypocenter depth $H \leq 160$ km.

- \mathbf{S}_1 is the 3D field of the density of earthquake epicenters.
- \mathbf{S}_2 is the 3D field of the mean earthquake magnitude.
- \mathbf{S}_3 is the 3D field of the negative temporal anomalies of the density of earthquake epicenters.
- \mathbf{S}_4 is the 3D field of the positive temporal anomalies of the density of earthquake epicenters.
- \mathbf{S}_5 is the 3D field of the negative temporal anomalies of the mean earthquake magnitude.
- \mathbf{S}_6 is the 3D field of the positive temporal anomalies of the mean earthquake magnitude.
- \mathbf{S}_7 is the 2D field of the density of earthquake epicenters: Kernel smoothing with the parameter $R = 50$ km in the interval from the beginning of the analysis to the start of training.
- \mathbf{S}_8 is the 3D field of quantiles of the background density of earthquake epicenters, calculated using the interval from the beginning of the analysis to the start of training, which corresponds to the density values of earthquake epicenters at the current time.

The estimation of 3D fields \mathbf{S}_1 and \mathbf{S}_2 was performed with the method of local kernel regression. The kernel function for the q -th earthquake has the form $K_q = [ch^2(r_q/R)^2ch^2(t_q/T)]^{-1}$, where $r_q < R\epsilon$ and $t_q < T\epsilon$ are the distance and time interval between the q -th epicenter of the earthquake and the node of the

3D grid of the field, $\epsilon = 2$, $R = 50$ km, $T = 100$ days for \mathbf{S}_1 and $R = 100$ km, and $T = 730$ days for \mathbf{S}_2 . The field \mathbf{S}_7 was calculated with the kernel function $K_q = [\cosh^2(r_q/R)^2]^{-1}$. The parameters for evaluating the fields, the radii R , and the interval T were chosen empirically, considering the step of the network of fields and the approximate number of events in the evaluation window. To calculate the fields \mathbf{S}_3 , \mathbf{S}_4 , \mathbf{S}_5 , and \mathbf{S}_6 , Student's t -test was used. This t -statistic was determined for each grid node as the ratio of the difference in the average values of the current interval T_2 and the background interval T_1 to the standard deviation of this difference. Positive values of the t -statistic correspond to an increase in the value on the test interval.

We also analyzed fields similar to the fields \mathbf{S}_3 , \mathbf{S}_4 , \mathbf{S}_5 , and \mathbf{S}_6 , but with different values of the T_2 and T_1 intervals.

When predicting from seismological data, the following three fields turned out to be the most informative.

- $\mathbf{S}_9 = \mathbf{S}_1/(\mathbf{S}_8 + 0.001)$ is the field of ratios of the density values of the earthquake epicenters s_{1n} to the values of the quantiles of the density of the epicenters calculated on the interval from the beginning of the analysis to the start of training, which corresponds to the density values of earthquake epicenters at the current time ($s_{8n} + 0.001$).
- \mathbf{S}_{10} is the field of negative anomalies of Student's t -statistic of the density of earthquake epicenters with the intervals $T_1 = 1095$ and $T_2 = 365$ days.
- \mathbf{S}_{11} is the field of negative anomalies of Student's t -statistic of the mean earthquake magnitude with the intervals $T_1 = 1095$ and $T_2 = 730$ days.

For Japan, the most informative were the fields \mathbf{S}_9 and \mathbf{S}_{10} . Both of them previously proved to be the most effective in predicting earthquakes and their magnitudes in Kamchatka and the Aegean region. The anomalous values of the \mathbf{S}_9 field correspond to areas of the seismic process in which the density values of earthquake epicenters are quite high but significantly less than the average values of the density of epicenters in the interval from the beginning of the analysis to the start of training. The anomalous values of the \mathbf{S}_{10} field correspond to the spatio-temporal regions of the seismic process, in which the average values of the density of earthquake epicenters in the T_2 interval are significantly lower than the average field values in the T_1 interval. These changes highlight anomalous areas in which a quiescence sets in after the activation of the seismic process. The time series of the \mathbf{S}_{10} field simulates the preparation of strong earthquakes proposed by the AUF model proposed in [7]. For California, the most informative were the fields \mathbf{S}_9 and \mathbf{S}_{11} .

3.3 Earthquake Forecast

The training intervals start for Japan and California on 01.01.2011 and 23.12.2009 and end before the next forecast, starting on 20.11.2015 and 19.01.2013. Testing intervals are 20.11.2015–10.09.2020 for Japan and 19.01.2013–14.11.2020 for California. The areas of analysis at the testing intervals contain 14 epicenters of target earthquakes in Japan with a magnitude of

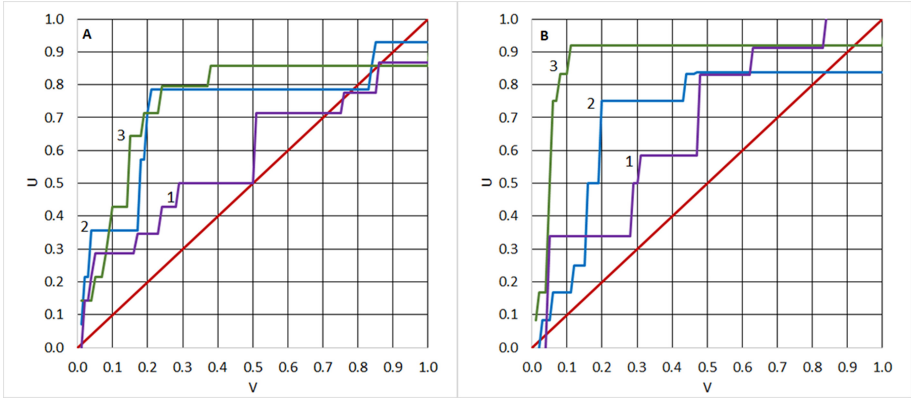


Fig. 2. Dependences $U(V)$ of the probability of a successful earthquake prediction U on the alarm volume V obtained with the different fields for Japan (A) and California (B). (1) field \mathbf{S}_7 for both regions; (2) fields \mathbf{S}_9 and \mathbf{S}_{10} for Japan, \mathbf{S}_9 and \mathbf{S}_{11} for California; (3) fields \mathbf{S}_9 , \mathbf{S}_{10} and \mathbf{F}_{10} for Japan, \mathbf{S}_9 , \mathbf{S}_{11} , \mathbf{F}_4 and \mathbf{F}_6 for California.

$m \geq 6.0$ and 12 epicenters of target earthquakes in California with a magnitude of $m \geq 5.5$.

In the method of the minimum area of alarm, alarm zones are constructed from a combination of spatio-temporal alarm cylinders. The parameters of the learning algorithm are the radius of the cylinders in spatial coordinates and the element of the cylinder in time. The larger the radius, the higher the alarm volume V . The larger the element, the slower the alarm zone changes. The alarm cylinder parameters are the radius $R = 16$ km and its element $T = 91$ days for Japan and $R = 18$ km and its element $T = 61$ days for California. The best forecast of target earthquakes according to GPS data for Japan was obtained from the \mathbf{F}_{10} field, and for California from the \mathbf{F}_4 and \mathbf{F}_6 fields.

Figure 2 shows the dependences $U(V)$ for Japan (A) and California (B). The results for Japan obtained using 2D field \mathbf{S}_7 of the density of earthquake epicenters (line 1), seismological fields \mathbf{S}_9 , \mathbf{S}_{10} (line 2), and the fields \mathbf{S}_9 , \mathbf{S}_{10} with the field \mathbf{F}_{12} (line 3). The result of forecasting earthquakes in California obtained using field \mathbf{S}_7 , fields \mathbf{S}_9 and \mathbf{S}_{11} , and fields \mathbf{S}_9 , \mathbf{S}_{11} , with the fields \mathbf{F}_4 and \mathbf{F}_6 .

4 Conclusion

A number of seismically active regions are equipped with a rather dense network of GPS receiving stations that track the movements of the earth’s surface. In our study, we tried to get answers to two questions: (1) Is space geodesy data effective for systematic earthquake prediction? and (2) Is the earthquake forecast improved if seismological data with the addition of space geodesy data? Obviously, the answers to these questions depend on the spatial density of the

network of receiving stations, on the parameters of the time series of GPS measurements, on the method of preprocessing of GPS data, and on the method for forecasting earthquakes.

The results in this article are based on data for the Japan and California regions. Our data from space geodesy are represented by daily time series of horizontal displacements of the earth's surface. The GPS time series processing is based on the calculation of the spatio-temporal fields of changes in the seismic strain rate invariants. To predict earthquakes, we used our method of the minimum area of alarm. It is shown that the probability of predicting earthquakes based on combined GPS and seismological data is almost the same as a forecast based only on seismological data in Japan and much higher in California.

A number of transformations were required to calculate feature fields based on GPS data. These include interpolation of time series at relatively small time intervals of discontinuity in the operation of GPS receiving stations, calculation of time series of the components of the velocities of horizontal displacements of stations, calculation of spatio-temporal fields of components of the velocities of the earth's surface deformations, calculation of fields of invariants of velocities and fields of variation of invariants of velocities in time, calculation of spatial correlation fields, calculation of minimum and maximum values of correlations, etc. A number of parameters were used in the algorithms for calculating these transformations: the time interval for estimating the daily displacement rates, the sizes of the spatial and temporal smoothing windows and the windows for estimating the spatial correlation coefficients, as well as the time intervals for calculating the field of invariants of the strain rates. The GPS fields for Japan and California were calculated with the same parameters. The choice of transformation parameters, as well as the choice of the feature fields themselves, requires special studies. In this work, such studies were not carried out. The types of transformations of the initial data into the fields of features and transformation parameters were selected based on qualitative considerations about the methods of cleaning signals from noise, recovering missing values, and disclosing information about the spatio-temporal properties of geodynamic processes.

The method of the minimum area of alarm is universal for various types of initial data since, for forecasting, all data is converted into uniform spatial, and spatio-temporal grid-based fields. The most informative for predicting earthquakes were the fields reflecting the change in the rates of various types of deformations of the earth's surface, the change in the characteristics of the seismic regime and the spatial correlation of these processes. The modeling of the earthquake prediction in the regions under study showed that these fields' anomalous values distinguish the spatio-temporal regions preceding the appearance of the epicenters of strong earthquakes. This is the similarity of the most informative feature fields selected for forecasting in the regions of Japan and California. It should be noted that these regions differ significantly in seismotectonic and geodynamic regimes [5, 19]. This testifies in favor of the universality of the proposed methods of our data preprocessing.

References

1. Barnhart, W.D., Hayes, G.P., Wald, D.J.: Global earthquake response with imaging geodesy: recent examples from the USGS NEIC. *Remote Sens.* **11**(11), 1357 (2019)
2. Bishop, C.M.: *Pattern Recognition and Machine Learning*. Springer, Heidelberg (2006)
3. Blewitt, G., Hammond, W.C., Kreemer, C.: Harnessing the GPS data explosion for interdisciplinary science. *Eos* **99**(10.1029) (2018)
4. Dobrovolsky, I., Zubkov, S., Miachkin, V.: Estimation of the size of earthquake preparation zones. *Pure Appl. Geophys.* **117**(5), 1025–1044 (1979)
5. Garagash, I., Bondur, V., Gokhberg, M., Steblov, G.: Three-year experience of the fortnight forecast of seismicity in Southern California on the basis of geomechanical model and the seismic data. In: *AGU Fall Meeting Abstracts*, vol. 2011, pp. NH23A-1535 (2011)
6. Geller, R.J., Jackson, D.D., Kagan, Y.Y., Mulargia, F.: Earthquakes cannot be predicted. *Science* **275**(5306), 1616 (1997)
7. Gitis, V., Derendyaev, A.: The method of the minimum area of alarm for earthquake magnitude prediction. *Front. Earth Sci.* **8**, 482 (2020)
8. Gitis, V.G., Derendyaev, A.B.: Machine learning methods for seismic hazards forecast. *Geosciences* **9**(7), 308 (2019)
9. Gufeld, I.L., Matveeva, M.I., Novoselov, O.N.: Why we cannot predict strong earthquakes in the earth's crust. *Geodyn. Tectonophys.* **2**(4), 378–415 (2015)
10. Guomin, Z., Zhaocheng, Z.: The study of multidisciplinary earthquake prediction in China. *J. Earthq. Prediction Res.* **1**(1), 71–85 (1992)
11. Kanamori, H.: The nature of seismicity patterns before large earthquakes (1981)
12. Keilis-Borok, V., Soloviev, A.A.: *Nonlinear Dynamics of the Lithosphere and Earthquake Prediction*. Springer, Heidelberg (2013)
13. Khan, S.S., Madden, M.G.: A survey of recent trends in one class classification. In: Coyle, L., Freyne, J. (eds.) *AICS 2009. LNCS (LNAI)*, vol. 6206, pp. 188–197. Springer, Heidelberg (2010). https://doi.org/10.1007/978-3-642-17080-5_21
14. King, C.Y.: Gas geochemistry applied to earthquake prediction: an overview. *J. Geophys. Res. Solid Earth* **91**(B12), 12269–12281 (1986)
15. Koronovsky, N., Naimark, A.: Earthquake prediction: is it a practicable scientific perspective or a challenge to science? *Mosc. Univ. Geol. Bull.* **64**(1), 10–20 (2009)
16. Kossobokov, V.: User manual for M8. In: Healy, J.H., Keilis-Borok, V.I., Lee, W.H.K. (eds.) *Algorithms for Earthquake Statistics and Prediction*, vol. 6, pp. 167–222 (1997)
17. Kotsiantis, S.B., Zaharakis, I., Pintelas, P.: Supervised machine learning: a review of classification techniques. *Emerg. Artif. Intell. Appl. Comput. Eng.* **160**(1), 3–24 (2007)
18. Lighthill, J.: *A Critical Review of VAN: Earthquake Prediction from Seismic Electrical Signals*. World Scientific (1996)
19. Lobkovsky, L., Vladimirova, I., Gabsatarov, Y.V., Steblov, G.: Seismotectonic deformations related to the 2011 Tohoku earthquake at different stages of the seismic cycle, based on satellite geodetic observations. *Doklady Earth Sci.* **481**, 1060–1065 (2018)
20. Mogi, K.: Two kinds of seismic gaps. *Pure Appl. Geophys.* **117**(6), 1172–1186 (1979)
21. Obara, K., Kasahara, K., Hori, S., Okada, Y.: A densely distributed high-sensitivity seismograph network in Japan: Hi-net by national research institute for earth science and disasterprevention. *Rev. Sci. Instrum.* **76**(2), 021301 (2005)

22. Okada, Y., et al.: Recent progress of seismic observation networks in Japan-Hi-net, F-net, K-net and KiK-net. *Earth Planets Space* **56**(8), xv–xxviii (2004)
23. Rhoades, D.A.: Application of the EEPAS model to forecasting earthquakes of moderate magnitude in southern California. *Seismol. Res. Lett.* **78**(1), 110–115 (2007)
24. Rhoades, D.A.: Mixture models for improved earthquake forecasting with short-to-medium time horizons. *Bull. Seismol. Soc. Am.* **103**(4), 2203–2215 (2013)
25. Shebalin, P.N., Narteau, C., Zechar, J.D., Holschneider, M.: Combining earthquake forecasts using differential probability gains. *Earth Planets Space* **66**(1), 1–14 (2014). <https://doi.org/10.1186/1880-5981-66-37>
26. Sobolev, G.: Principles of earthquake prediction (1993)
27. Sobolev, G., Ponomarev, A.: *Earthquake Physics and Precursors*. Publishing House Nauka, Moscow (2003)
28. Zadeh, L.A.: Fuzzy logic. *Computer* **21**(4), 83–93 (1988)
29. Zavyalov, A.: *Intermediate Term Earthquake Prediction*. Nauka, Moscow (2006)
30. Zhang, L.Y., Mao, X.B., Lu, A.H.: Experimental study of the mechanical properties of rocks at high temperature. *Sci. China Ser. E* **52**(3), 641–646 (2009)